Experimental demonstration of error-insensitive approximate universal-NOT gates

Sang Min Lee,[1] Jeongho Bang,[2] Heonoh Kim,[1] Hyunseok Jeong,[2] Jinhyoung Lee,[3] and Han Seb Moon[1,*]

[1]*Department of Physics, Pusan National University, Busan 609-735, Korea*

[2]*Center for Macroscopic Quantum Control, Department of Physics and Astronomy, Seoul National University, Seoul 151-747, Korea*

[3]*Department of Physics, Hanyang University, Seoul 133-791, Korea*

(Received 19 March 2014; published 28 May 2014)

We propose and experimentally demonstrate an approximate universal-NOT (UNOT) operation that is robust against operational errors. In our proposal, the UNOT operation is composed of stochastic unitary operations represented by the vertices of regular polyhedrons. The operation is designed to be robust against random operational errors by increasing the number of unitary operations (i.e., reference axes). Remarkably, no increase in the total number of measurements nor additional resources are required to perform the UNOT operation. Our method can be applied in general to reduce operational errors to an arbitrary degree of precision when approximating any antiunitary operation in a stochastic manner.

DOI: 10.1103/PhysRevA.89.052329 PACS number(s): 03.67.Pp, 03.67.Lx, 42.50.Ex, 42.50.Xa

I. INTRODUCTION

For the implementation of quantum information processing, it is necessary to reduce errors and their effects on whole processes. Quantum information processing such as quantum computing and communications is composed of three stages: state preparation, operations, and measurements. Any physical process that is described, either implicitly or explicitly, within the framework of quantum mechanics consists of these three stages and errors may occur during any processes. Errors are detrimental to the final outcome in the measurement stage: For example, both the decoherence process that changes the state before the final measurement and the inefficiency of the measurement device (i.e., detector) will affect the results. Recently, it was reported that the inaccuracy of unitary operations such as incorrect changes in the references for measurements plays a crucial role in diminishing quantum effects [1]. We refer to these types of errors as operational errors, in contrast to the errors caused by state decoherence or inefficient detection. Schemes including the composite pulse technique [2,3] and quantum error correction codes [4] have been suggested to reduce or correct various types of errors, but these methods require additional resources such as a larger number of pulses [3] or ancillary qubits [5] to enhance the precision of quantum information processing.

Antiunitary operations in quantum mechanics are nonphysical operations and thus they cannot be implemented in a perfect manner. However, approximate implementations are possible [6–8] and some implementations such as the universal-NOT (UNOT) gate [6] and the transpose operation [8] are particularly useful for quantum cloning, quantum state estimation, and entanglement detection [8–13]. The approaches taken for the implementation of antiunitary operations can be categorized into two types: ancilla-assisted models [6] and stochastic mapping [7,8], as outlined in [14]. The necessary condition for the universality of each approach has been shown to be two ancillary qubits or three stochastic operations.

There are two important factors for implementing a UNOT gate. One factor is the average value of the fidelities to the target state for all possible input states and the other is their standard deviation, known as the universality [14]. Typically, the average fidelity is the dominant factor when estimating the accuracy of a quantum operation. However, the fidelity deviation may also be important in some cases [15]. An approximate UNOT gate is one such example [6] in which the fidelity is $\frac{2}{3}$ for any input state so that the zero fidelity deviation is always guaranteed. In fact, there may be situations in which the fidelity deviation is practically important. For example, certain tasks such as fault-tolerant quantum computing [16] may require the fidelity to be above a certain limit. In addition, supposing that an ensemble of a pure state is the input for a quantum operation but we do not know which pure state it is in (the input is an unknown state), then it may be important to reduce the fidelity deviation, i.e., the sensitivity of the final results to the input state or operational errors.

In this paper we propose and experimentally demonstrate a method to effectively reduce the effects of operational errors on the operation of an approximate UNOT gate. The UNOT gate is designed to be insensitive to operational errors by increasing the number of reference axes without increasing any resources or the total number of measurements. The experiment in this study was performed for stochastic mapping, but the same method is applicable to a certain ancilla-assisted model. We used spontaneous parametric down-conversion (SPDC) and linear optics elements in the experimental realization and the stochastic map was characterized by quantum process tomography (QPT) [4]. From the results of the QPT, we calculated the sensitivities of the maps, which matched well with the simulations and analytic predictions. In principle, our method to reduce the effects of operational errors can be applied to any type of approximate antiunitary operation realized in a stochastic manner.

II. CONCEPT AND THEORY

The UNOT gate is represented by the mapping $|\psi\rangle \mapsto |\psi_\perp\rangle$, where $|\psi\rangle$ is an arbitrary unknown input state in a qubit and $|\psi_\perp\rangle$ is its orthogonal state. It is well known that such a gate cannot be completely realized, but only approximately implemented [6]. To evaluate the approximate UNOT gate, we introduce two measures, the average fidelity F and fidelity

*moon.hanseb@gmail.com

deviation Δ, defined as

$$F = \int f(\psi)d\psi, \quad \Delta = \sqrt{\int f(\psi)^2 d\psi - F^2}, \tag{1}$$

where $f(\psi)$ is the fidelity between the orthogonal state and the output state of the approximate operation O for a pure input state $|\psi\rangle$, i.e., $f(\psi) = \langle\psi_\perp|O(\psi)|\psi_\perp\rangle$. Note that F can be maximized to $\frac{2}{3}$ (the so-called optimality condition) and Δ can be 0 (the so-called universality condition); these are regarded as the best conditions for realizing an optimum approximate UNOT gate.

In Ref. [14], it was demonstrated that the approximate UNOT gate can be realized with three or more stochastic unitary operations such that $\rho \mapsto O(\rho) = \sum_{i=1}^{m} p_i U_i \rho U_i^\dagger (m \geqslant 3)$, where U_i is a single-qubit unitary operation given by $U_i = \cos\frac{\theta_i}{2} I + \sin\frac{\theta_i}{2}(\vec{\sigma}\cdot\vec{n}_i)$. Here $\vec{\sigma} = (\sigma_1,\sigma_2,\sigma_3)$ is a vector operator whose elements are the Pauli operators, $\vec{n}_i = (n_{i1},n_{i2},n_{i3})$ is a normalized (real) vector, i.e., $|\vec{n}_i| = 1$, and $\{p_i\}$ is the probability distribution of the stochastic operations such that $\sum p_i = 1$. The necessary condition for obtaining the maximum F is that the rotation angles $\{\theta_i\}$ are π (for all $i = 1,2,\ldots,m$). However, perfect universality (i.e., $\Delta = 0$) is achieved by choosing an appropriate set of normalized directional vectors $\{\vec{n}_i\}$ and a suitable probability distribution $\{p_i\}$. We find conditions of $\{\vec{n}_i\}$ for a uniform distribution of $\{p_i\}$: $\{\vec{n}_i\}$ point to the vertices of regular polyhedrons [17] that are equally distributed in a solid angle. Based on the above descriptions, our generalized stochastic process for the approximate UNOT operation is as follows:

$$\rho \to \rho'_N = O_N(\rho) = \frac{1}{N}\sum_{i=1}^{N}(\vec{\sigma}\cdot\vec{n}_i)\rho(\vec{\sigma}\cdot\vec{n}_i). \tag{2}$$

For the cases of O_3 and O_4, the $\{\vec{n}_i\}$ are given by $\{(1,0,0),(0,1,0),(0,0,1)\}$ and $\{(\frac{1}{\sqrt{3}},\frac{1}{\sqrt{3}},\frac{1}{\sqrt{3}}),(\frac{1}{\sqrt{3}},\frac{-1}{\sqrt{3}},\frac{-1}{\sqrt{3}}),(\frac{-1}{\sqrt{3}},\frac{1}{\sqrt{3}},\frac{-1}{\sqrt{3}}),(\frac{-1}{\sqrt{3}},\frac{-1}{\sqrt{3}},\frac{1}{\sqrt{3}})\}$, which correspond to the vertices of an octahedron and a tetrahedron, respectively. We can easily generalize these to the cases of O_6 and O_8 by considering the opposite directional vectors $\{-\vec{n}_i\}$. If error-free (in the ideal case), all the maps O_N in Eq. (2) are equivalent to that of $N = 3$, the Hillery-Bužek UNOT gate [18,19] as $\rho \mapsto O_I(\rho) = \frac{1}{3}(\sigma_x\rho\sigma_x + \sigma_y\rho\sigma_y + \sigma_z\rho\sigma_z)$. Thus, Eq. (2) is the optimum approximate UNOT gate.

We now consider the maps O_N with errors by taking realistic circumstances into account. Errors usually deteriorate the average fidelity and fidelity deviation in implementations of the approximate UNOT gate and here we consider a specific but very common (operational) error that arises from the imperfect setting of U_i. It is important to note that Δ can be seriously affected by even a small error, whereas F will remain close to its maximum value of $\frac{2}{3}$ [14]. This trend motivated us to invent an error-insensitive approximate UNOT gate, significantly reducing the influence of the errors on Δ.

We show that adding more stochastic operations will increase the resilience against the operational errors. This can be verified by analytic calculations for the cases of $N = 3$, 4, 6, and 8. The process in Eq. (2) is characterized by χ matrices through $O(\rho) = \sum_{i,j=0}^{3}\chi_{ij}\sigma_i\rho\sigma_j$, where $\sigma_0 = I$ [4], and so the ideal case of the approximate UNOT gate is characterized by $\chi_I = \mathrm{diag}(0,\frac{1}{3},\frac{1}{3},\frac{1}{3})$. However, operational errors occurring under realistic circumstances will vary χ_I. By using the χ matrix, we can find the mean of average fidelity $\overline{F}_N$ and fidelity deviation $\overline{\Delta}_N$ for the map O_N over the random errors as

$$\overline{F}_N \simeq \frac{2}{3}, \quad \overline{\Delta}_N \simeq \frac{\alpha}{\sqrt{N}}\delta_r = \mathcal{S}_N\delta_r, \tag{3}$$

where α is a constant factor and δ_r is the standard deviation of the random error. Since $\overline{F}_N$ is stationary, we define the error sensitivity of O_N with $\overline{\Delta}_N$ as $\mathcal{S}_N \equiv \alpha/\sqrt{N}$ (see Appendix C for more details). In deriving Eq. (3), the random error is considered as a random unitary operation V_i following the stochastic operation, e.g., $\vec{\sigma}\cdot\vec{n}_i \xrightarrow{\text{error}} V_i(\vec{\sigma}\cdot\vec{n}_i)$. We consider the error operation as $V_i = e^{i\vec{\epsilon}_i\cdot\vec{\sigma}} \simeq I + i\vec{\epsilon}_i\cdot\vec{\sigma}$, where $\vec{\epsilon}_i = (\epsilon_{i1},\epsilon_{i2},\epsilon_{i3})$ and $|\epsilon_{ij}| < \epsilon_0 \ll 1$, so that the error distribution is symmetric and homogeneous (see Appendix B for more details). Equation (3) shows directly that the deterioration of Δ_N due to operational errors can be reduced by simply increasing the number of stochastic operations N.

Note that N is the number of stochastic operations that constitute the map O_N and is not the number of measurements. However, we see that Eq. (3) is very similar in form to that for the standard error of N measurements of random variables. The reason for this similarity is that the output state of the map is a mixed state: a convex combination of N states. An erroneous output state of O_N is expressed as a summation of vectors in the Bloch sphere as $\sum_{i=1}^{N}(\vec{o}_i + \vec{e}_i)/N$, where $\vec{o}_i$ are the Bloch vectors of ideal stochastic operations and $\vec{e}_i$ are effects of the operational errors [20]. The total effect of operational errors is described as $\sum_{i=1}^{N}\vec{e}_i/N$ with an average of zero and a standard deviation proportional to $\Delta(|\vec{e}_i|)/\sqrt{N}$. Therefore, the average fidelity remains close to the maximum and a mean of Δ_N for an erroneous map is expressed by Eq. (3).

III. SETUP AND METHOD

The experiment was based on the polarization state of a single photon generated from SPDC and manipulated by linear

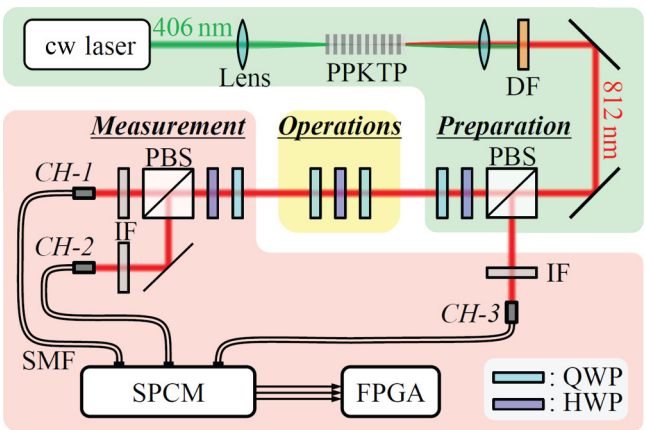

FIG. 1. (Color online) Experimental setup: PPKTP, periodically poled potassium titanyl phosphate ($KTiOPO_4$); DF, dichroic filter; PBS, polarizing beam splitter; QWP, quarter-wave plate; HWP, half-wave plate; IF, interference filter; CH-1(2), polarization analyzer channel; CH-3, counting trigger channel for coincidence counts; SMF, single-mode fiber; SPCM, single photon counting modules; and FPGA, coincidence counter.

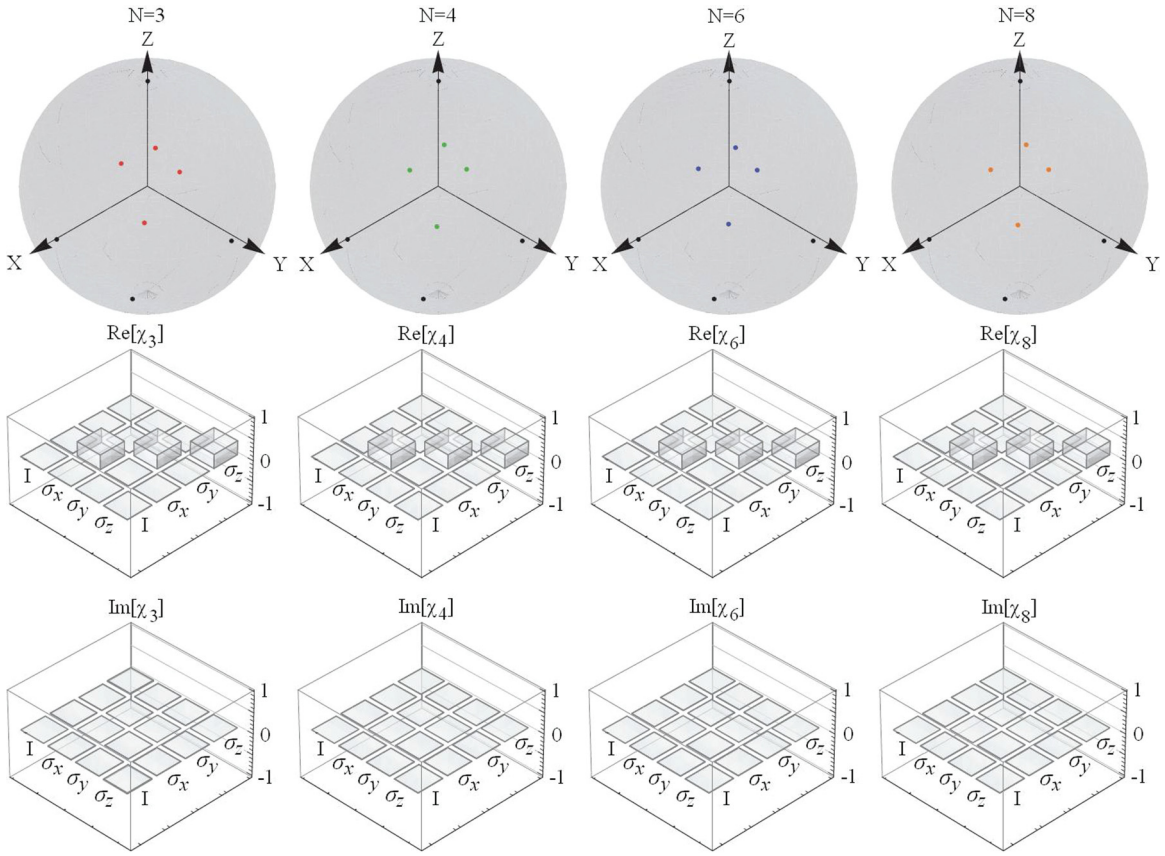

FIG. 2. (Color online) Experimentally reconstructed input and output states of the maps $O_{3,4,6,8}$ for QPT and their χ matrices under error-free circumstances.

optics, as shown in Fig. 1. We first generated a pair of photons via a frequency-degenerate collinear type-II SPDC process using a diode continuous-wave laser (1.8 mW at 406 nm) and a periodically poled $KTiOPO_4$ crystal ($L = 10$ mm, $\Lambda = 10.00$ μm). The polarizations of the two photons in a single mode (the same frequency and spatial mode) were orthogonal to each other as $|HV\rangle$. A horizontal photon transmitting the polarizing beam splitter (PBS) was controlled to be in an arbitrary polarization qubit state through the use of the half-wave plate (HWP) and the quarter-wave plate (QWP). The vertical photon plays the role of a counting trigger for coincidence counts.

An arbitrary unitary operation for the polarization qubit can be realized by a set of wave plates (QWP-HWP-QWP) [21]. We stochastically perform unitary operations $\{\vec{\sigma} \cdot \vec{n}_i\}$ to realize the map O_N. The random error of a unitary operation is achieved by rotating each wave plate in the set randomly between $[-\phi_e, \phi_e]$.

The output states are measured by a polarization analyzer (QWP-HWP-PBS) and reconstructed by quantum state tomography (QST) [22]. To obtain F_N, Δ_N, and $\mathcal{S}_N$ of each stochastic map O_N, we execute QPT, which characterizes a quantum operation by means of the QST results for four input states and their output states. From the result of QPT and χ matrix, we can calculate F_N and Δ_N (see Appendix A for more details). To survey $\mathcal{S}_N$, we repeat the QPT measurements of O_N for $N = 3$, 4, 6, and 8 by varying the boundaries of the random error ϕ_e from 0° to 5° [23].

IV. RESULTS AND ANALYSIS

Figure 2 shows reconstructed input states and their output states for QPTs of the maps $O_{3,4,6,8}$ in the Bloch spheres [24] and χ_N matrices when there are no operational errors. The points (in black) on the surface are the input states and the points (in red, green, blue, and orange) close to the center represent the output states of the maps $O_{3,4,6,8}$ [25]. The graphs show clearly that the output states are on opposite sides of the input states and that their lengths decrease by about $\frac{1}{3}$. The χ_N matrices are calculated from the reconstructed density matrices of the input and output states and these are almost the same as those of the ideal case, i.e., $\chi_{11} = \chi_{22} = \chi_{33} = \frac{1}{3}$. This constitutes experimental verification of the equivalence of the maps O_N for $N = 3, 4, 6$, and 8 under error-free circumstances.

Figure 3 represents the input and output states of erroneous maps $O^{\text{err}}_{3,4,6,8}$ for $\phi_e = 5°$ [24]. The output states of O^{err}_N are more diffused than those of O^{err}_M, where $N < M$, and we see that for larger N, the map O_N is less sensitive to random operational errors. Since the output states have a distribution in the Bloch sphere, we describe the erroneous maps O^{err}_N as the average value of F_N and Δ_N over 20 QPT results.

We repeated the QPT experiments for the maps $O^{\text{err}}_{3,4,6,8}$ for various error boundaries ϕ_e to measure $\mathcal{S}_N$. The average values of F_N and Δ_N for random errors are shown in Fig. 4. Each point represents the average value of 20 experimental results, except for the error-free case ($\phi_e = 0°$) in which two results were averaged. The solid and dashed lines represent linear fits

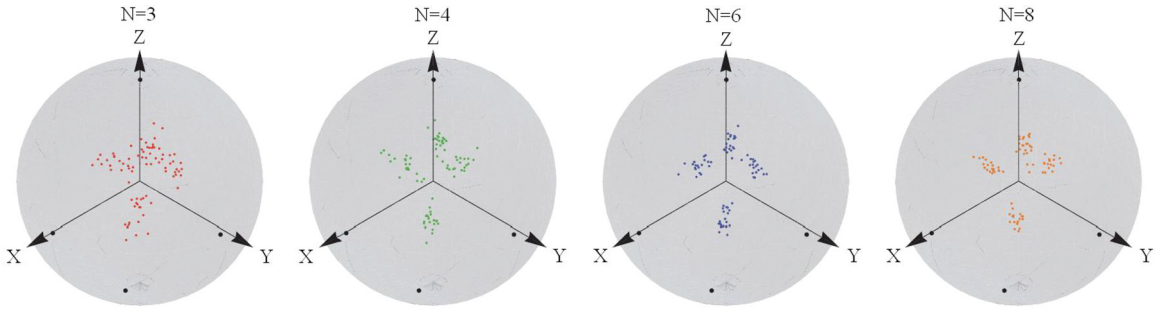

FIG. 3. (Color online) Experimentally reconstructed input and output states of erroneous maps $O^{\text{err}}_{3,4,6,8}$ when $\phi_e = 5^\circ$.

of the experimental data and trends of the simulation results for 10^4 QPT measurements, respectively. The simulation results are shifted up about 0.005 to match the experimental results. We attribute this offset to inevitable imperfections in the experimental setup and measurements.

In Fig. 4 the results of $\overline{\Delta}_N$ are distinct for different N, although there are no significant differences in $\overline{F}_N$. The experimental data of $\overline{\Delta}_N$ and $\overline{F}_N$ agree well with the simulation results to within the deviations. From Eq. (3) we note that the gradients of the $\overline{\Delta}_N$ curves corresponding to the sensitivity $\mathcal{S}_N$ and the relative gradients $\mathcal{S}_N/\mathcal{S}_M$ obtained from the experimental data (simulation results) for $\overline{\Delta}_N$ and $\overline{\Delta}_M$ obey the relation $\sqrt{M/N}$ to within an accuracy of about 82% (99%). This shows that the sensitivity of the stochastic map O_N is inversely proportional to the square root of the number of operations N as described in Eq. (3).

Note that all the experimental data (one QST or one QPT) were measured using the same amount of resources (photon pairs). Thus, the error insensitivity of O_N is not a matter of the measurement precision dependent on the number of repetitions. The essential point of our scheme is that the output state is a convex combination of other states, so we expect that our error-insensitive method will be applicable to other stochastic operations. We utilized the stochastic method rather than the ancilla-assisted model, which demands $N-1$ controlled unitary operations for O_N, so as to avoid any controlled unitary operations that are probabilistic in the framework of linear optics. Most cases of the ancilla-assisted model are composed of sequential controlled unitary operations so that their operational errors can be accumulated. Therefore, to apply our method to the ancilla-assisted model, a specific controlled operation and an equally superposed ancilla state are required, e.g., $U^{(N)}_{AB} = \sum_{i=1}^{N} |i\rangle_A\langle i| \otimes (\vec{\sigma}\cdot\vec{n}_i)_B$ and $|\psi_0\rangle_A = \frac{1}{\sqrt{N}}\sum_{i=1}^{N}|i\rangle$, where A and B denote ancilla and object systems, respectively.

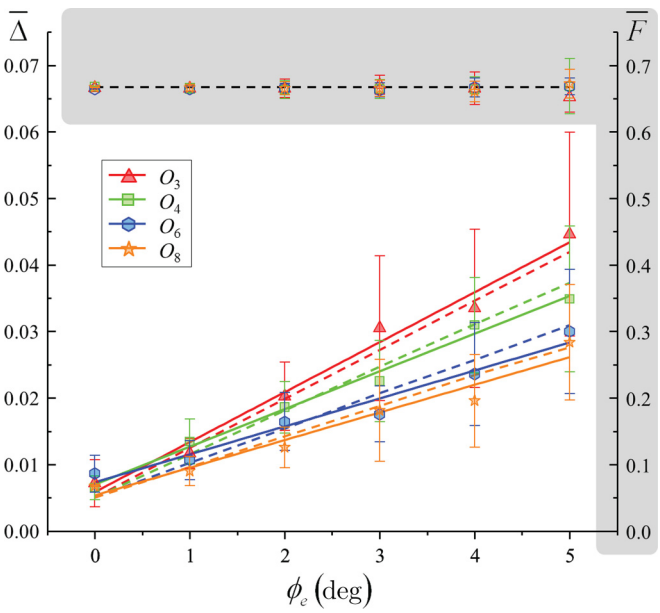

FIG. 4. (Color online) Average values of F_N and Δ_N for $O^{\text{err}}_{3,4,6,8}$ for various random error boundaries ϕ_e. The points and solid lines are the averages of the experimental results and a linear fit of the data. The dashed lines are shifted trends of the simulation results for 10^4 QPT measurements.

V. CONCLUSION

We have introduced an error-insensitive (robust) UNOT gate consisting of stochastic unitary operations with rotation axes corresponding to the vertex directions of an octahedron and hexahedron and a rotation angle of π. We demonstrated both theoretically and experimentally that the sensitivity of the map to random operational errors is inversely proportional to the square root of the number of stochastic operations. The method does not require any increase in the total number of measurements nor additional resources. Even though we have considered only the maps O_N for $N = 3, 4, 6$, and 8, our scheme can be generalized to $N = 3n$ and $4n$ $(1 \leqslant n)$. This method is also applicable to all approximate antiunitary operations, since such operations are equivalent to a unitary transformation, and it may be possible to extend the method to other stochastic mappings.

ACKNOWLEDGMENTS

S.M.L. and H.S.M. thank Hee Su Park for fruitful discussions. This research was supported by the Basic Science Research Program through the National Research Foundation of Korea funded by the Ministry of Education, Science and Technology (Grants No. 2012R1A2A1A01006579, No. 2013R1A4A1069587, No. 2010-0015059, and No. 2010-0018295).

APPENDIX A: CALCULATION OF F AND Δ FROM THE χ MATRIX

When a quantum operation O is characterized by a χ matrix as

$$\chi = \begin{pmatrix} \chi_{11} & \chi_{12} & \chi_{13} & \chi_{14} \\ \chi_{12}^* & \chi_{22} & \chi_{23} & \chi_{24} \\ \chi_{13}^* & \chi_{23}^* & \chi_{33} & \chi_{34} \\ \chi_{14}^* & \chi_{24}^* & \chi_{34}^* & \chi_{44} \end{pmatrix}, \tag{A1}$$

the output state is expressed as

$$O(\psi) = \sum_{i,j=0}^{3} \chi_{ij}\sigma_i|\psi\rangle\langle\psi|\sigma_j, \tag{A2}$$

where σ_0 is 2×2 identity matrix and $\sigma_{i\neq 0}$ are the Pauli matrices. The fidelity between the output state of the map O and ideal UNOT gate is described as

$$\begin{aligned} f(O(\psi),\psi_\perp) &= \langle\psi_\perp|O(\psi)|\psi_\perp\rangle \\ &= \sum_{i,j=0}^{3} \chi_{ij}\langle\psi_\perp|\sigma_i|\psi\rangle\langle\psi|\sigma_j|\psi_\perp\rangle \\ &= \sum_{i,j=0}^{3} \chi_{ij}C_iC_j^*, \end{aligned} \tag{A3}$$

where the coefficients are defined as $C_i \equiv \langle\psi_\perp|\sigma_i|\psi\rangle$. Since an arbitrary pure state and its orthogonal state can be represented by $|\psi\rangle = \cos\frac{\theta}{2}|0\rangle + e^{i\phi}\sin\frac{\theta}{2}|1\rangle$ and $|\psi_\perp\rangle = \sin\frac{\theta}{2}|0\rangle - e^{i\phi}\cos\frac{\theta}{2}|1\rangle$, respectively, where $\theta = [0,\pi]$ and $\phi = [0,2\pi]$, the coefficients C_i are functions of θ and ϕ. Thus, the average fidelity F and the square of the fidelity deviation Δ^2 are obtained as

$$\begin{aligned} F &= \frac{1}{4\pi}\sum_{i,j=0}^{3}\chi_{ij}\iint C_iC_j^*\sin\theta\, d\theta\, d\phi \\ &= \frac{2}{3}(\chi_{11}+\chi_{22}+\chi_{33}), \end{aligned} \tag{A4}$$

$$\begin{aligned} \Delta^2 &= \frac{1}{4\pi}\sum_{i,j,k,l=0}^{3}\chi_{ij}\chi_{kl}\iint C_iC_j^*C_kC_l^*\sin\theta\, d\theta\, d\phi - F^2 \\ &= \frac{4}{45}\left(\chi_{11}^2+\chi_{22}^2+\chi_{33}^2-\chi_{11}\chi_{22}-\chi_{11}\chi_{33}-\chi_{22}\chi_{33}\right) \\ &\quad + \frac{4}{15}\left(3|\chi_{12}|^2+3|\chi_{13}|^2+3|\chi_{23}|^2\right. \\ &\quad \left. - 2\,\mathrm{Re}\left[\chi_{12}^2+\chi_{13}^2+\chi_{23}^2\right]\right). \end{aligned} \tag{A5}$$

APPENDIX B: RANDOM OPERATIONAL ERROR AND O_N^{err}

A random operational error can be considered as an additional random unitary operation following the original operation $\vec{\sigma}\cdot\vec{n}_i \xrightarrow{\text{error}} V_i(\vec{\sigma}\cdot\vec{n}_i)$. The error operation is defined as $V_i = e^{i\vec{\epsilon}_i\cdot\vec{\sigma}} \simeq I + i\vec{\epsilon}_i\cdot\vec{\sigma}$, where $\vec{\epsilon}_i = (\epsilon_{i1},\epsilon_{i2},\epsilon_{i3})$ and $|\epsilon_{ij}| \leqslant \epsilon_0 \ll 1$. The distribution of errors $P(\vec{\epsilon}_i)$ is assumed to be homogeneous and symmetric under the inversion $P(\vec{\epsilon}_i) = P(-\vec{\epsilon}_i)$ so that $\overline{\vec{\epsilon}_i} = 0$. Then, the erroneous map O_N^{err} is expressed as

$$\rho \to \rho_N'' = O_N^{\mathrm{err}}(\rho) = \frac{1}{N}\sum_{i=1}^{N} V_i(\vec{\sigma}\cdot\vec{n}_i)\rho(\vec{\sigma}\cdot\vec{n}_i)V_i^\dagger. \tag{B1}$$

APPENDIX C: PROOF OF EQ. (3)

1. The case of O_3^{err}

The first order of error terms $\delta O_3^{(1)}$ for the map O_3^{err} and their additional contribution $\delta\chi_3^{(1)}$ to χ_I matrix are

$$\begin{aligned} \delta O_3^{(1)} = \frac{1}{3}[&i(\vec{\epsilon}_1\cdot\vec{\sigma})\sigma_x\rho\sigma_x + i(\vec{\epsilon}_2\cdot\vec{\sigma})\sigma_y\rho\sigma_y \\ &+ i(\vec{\epsilon}_3\cdot\vec{\sigma})\sigma_z\rho\sigma_z + \text{c.c.}], \end{aligned} \tag{C1}$$

$$\delta\chi_3^{(1)} = \frac{1}{3}\begin{pmatrix} 0 & i\epsilon_{11} & i\epsilon_{22} & i\epsilon_{33} \\ -i\epsilon_{11} & 0 & \epsilon_{23}-\epsilon_{13} & \epsilon_{12}-\epsilon_{32} \\ -i\epsilon_{22} & \epsilon_{23}-\epsilon_{13} & 0 & \epsilon_{31}-\epsilon_{21} \\ -i\epsilon_{33} & \epsilon_{12}-\epsilon_{32} & \epsilon_{31}-\epsilon_{21} & 0 \end{pmatrix}. \tag{C2}$$

Using Eqs. (A4), (A5), and (C2), the average fidelity and the fidelity deviation for O_3^{err} are obtained as

$$F_3 = \frac{2}{3}, \tag{C3}$$

$$\begin{aligned} \Delta_3 &= \frac{2\sqrt{(\epsilon_{13}-\epsilon_{23})^2+(\epsilon_{21}-\epsilon_{31})^2+(\epsilon_{12}-\epsilon_{32})^2}}{3\sqrt{15}} \\ &= \frac{2\sqrt{2}}{3\sqrt{15}}\sqrt{r_1^2+r_2^2+r_3^2}, \end{aligned} \tag{C4}$$

where $\{r_i\}$ are replaced random variables of $\{\epsilon_{ij}\}$ up to normalization factor $\sqrt{2}$. Note that the errors of which directions are parallel to the original operations, i.e., $\{\epsilon_{ii}\}$, do not contribute to the average fidelity and the fidelity deviation as shown in Eqs. (C2)–(C4). A mean of the fidelity deviation over random errors is proportional to the standard deviation of random variables,

$$\overline{\Delta}_3 = \sqrt{\frac{8}{15}}\frac{\delta_r}{\sqrt{3}}. \tag{C5}$$

where $\delta_r = \overline{r_i^2}^{1/2}$ and we assume $\overline{r_i} = 0$.

2. The case of O_4^{err}

After tedious calculations, the first order of error terms $\delta O_4^{(1)}$ and their contribution $\delta\chi_4^{(1)}$ to the χ_I matrix are expressed as

$$\begin{aligned} \delta O_4^{(1)} = -\frac{1}{12}\{&[\epsilon_{11}\sqrt{3}\sigma_z + \epsilon_{12}(\sigma_x-\sqrt{2}\sigma_y)]\rho(\sqrt{2}\sigma_x+\sigma_y) + [\epsilon_{21}\sqrt{3}\sigma_z + \epsilon_{22}(\sigma_x+\sqrt{2}\sigma_y)]\rho(-\sqrt{2}\sigma_x+\sigma_y) \\ &+ [\epsilon_{31}\sqrt{3}\sigma_x + \epsilon_{32}(\sqrt{2}\sigma_y+\sigma_z)]\rho(-\sigma_y+\sqrt{2}\sigma_z) + [\epsilon_{41}\sqrt{3}\sigma_x + \epsilon_{42}(-\sqrt{2}\sigma_y+\sigma_z)]\rho(-\sigma_y-\sqrt{2}\sigma_z) + \text{c.c.}\}, \end{aligned} \tag{C6}$$

$$\delta\chi_4^{(1)} = \frac{1}{12}\begin{pmatrix} 0 & 0 & 0 & 0 \\ 0 & 2\sqrt{2}(-\epsilon_{12}+\epsilon_{22}) & \epsilon_{12}+\epsilon_{22}+\sqrt{3}(\epsilon_{31}+\epsilon_{41}) & \sqrt{6}(-\epsilon_{11}+\epsilon_{21}-\epsilon_{31}+\epsilon_{41}) \\ 0 & \epsilon_{12}+\epsilon_{22}+\sqrt{3}(\epsilon_{31}+\epsilon_{41}) & 2\sqrt{2}(\epsilon_{12}-\epsilon_{22}+\epsilon_{32}-\epsilon_{42}) & -\sqrt{3}(\epsilon_{11}+\epsilon_{21})-\epsilon_{32}-\epsilon_{42} \\ 0 & \sqrt{6}(-\epsilon_{11}+\epsilon_{21}-\epsilon_{31}+\epsilon_{41}) & -\sqrt{3}(\epsilon_{11}+\epsilon_{21})-\epsilon_{32}-\epsilon_{42} & 2\sqrt{2}(-\epsilon_{32}+\epsilon_{42}) \end{pmatrix}. \quad \text{(C7)}$$

In this case, for a simple calculation, we neglect errors that are parallel to the original operations since the errors do not contribute to the first-order calculation as shown in the case of O_3^{err}. Using Eqs. (A4), (A5), (C7), and replaced random variables, F_4 and Δ_4 for O_4^{err} are obtained as

$$F_4 = \frac{2}{3}, \quad \text{(C8)}$$

$$\Delta_4 = \frac{1}{3\sqrt{30}}\sqrt{(\sqrt{3}\alpha_+ + \delta_+)^2 + 6(\alpha_- + \gamma_-)^2 + (\beta_+ + \sqrt{3}\gamma_+)^2 + 8(\beta_-^2 + \beta_-\delta_- + \delta_-^2)}$$
$$= \frac{\sqrt{2}}{3\sqrt{15}}\sqrt{R_1^2 + 3R_2^2 + R_3^2 + 3R_4^2 + R_5^2}, \quad \text{(C9)}$$

where the replaced variables are defined as

$$\alpha_\pm = \frac{\epsilon_{11} \pm \epsilon_{21}}{\sqrt{2}}, \quad \beta_\pm = \frac{\epsilon_{12} \pm \epsilon_{22}}{\sqrt{2}}, \quad \gamma_\pm = \frac{\epsilon_{31} \pm \epsilon_{41}}{\sqrt{2}}, \quad \delta_\pm = \frac{\epsilon_{32} \pm \epsilon_{42}}{\sqrt{2}}, \quad \text{(C10)}$$

$$R_1 = \frac{\sqrt{3}\alpha_+ + \delta_+}{2}, \quad R_2 = \frac{\alpha_- + \gamma_-}{\sqrt{2}}, \quad R_3 = \frac{\beta_+ + \sqrt{3}\gamma_+}{2},$$
$$R_4 = \frac{\beta_- + \delta_-}{\sqrt{2}}, \quad R_5 = \frac{\beta_- - \delta_-}{\sqrt{2}}. \quad \text{(C11)}$$

A mean of Δ_4 over random errors is obtained as

$$\overline{\Delta}_4 = \sqrt{\frac{8}{15}}\frac{\delta_r}{\sqrt{4}}. \quad \text{(C12)}$$

3. The cases of O_6^{err} and O_8^{err}

From tedious calculations, average fidelities are the same as $\frac{2}{3}$ and means of Δ_6 and Δ_8 over random errors are obtained as

$$\overline{\Delta}_6 = \sqrt{\frac{8}{15}}\frac{\delta_r}{\sqrt{6}}, \quad \text{(C13)}$$

$$\overline{\Delta}_8 = \sqrt{\frac{8}{15}}\frac{\delta_r}{\sqrt{8}}. \quad \text{(C14)}$$

From Eqs. (C5) and (C12)–(C14), we infer that the average of Δ_N (at least for the cases of $N = 3n, 4n$) over random errors is expressed as

$$\overline{\Delta}_N = \sqrt{\frac{8}{15}}\frac{\delta_r}{\sqrt{N}}. \quad \text{(C15)}$$

[1] H. Jeong, Y. Lim, and M. S. Kim, Phys. Rev. Lett. **112**, 010402 (2014).
[2] H. K. Cummins, G. Llewellyn, and J. A. Jones, Phys. Rev. A **67**, 042308 (2003).
[3] J. A. Jones, Phys. Rev. A **87**, 052317 (2013).
[4] M. A. Nielsen and I. L. Chuang, *Quantum Computation and Quantum Information* (Cambridge University Press, Cambridge, 2000).
[5] P. W. Shor, Phys. Rev. A **52**, R2493 (1995).
[6] F. De Martini, V. Bužek, F. Sciarrino, and C. Sias, Nature (London) **419**, 815 (2002).
[7] F. Sciarrino, C. Sias, M. Ricci, and F. De Martini, Phys. Rev. A **70**, 052305 (2004).
[8] H.-T. Lim, Y.-S. Ra, Y.-S. Kim, J. Bae, and Y.-H. Kim, Phys. Rev. A **83**, 020301 (2011).
[9] V. Bužek, M. Hillery, and R. F. Werner, Phys. Rev. A **60**, R2626 (1999).
[10] S. J. van Enk, Phys. Rev. Lett. **95**, 010502 (2005).
[11] F. Sciarrino and F. De Martini, Phys. Rev. A **76**, 012330 (2007).
[12] N. Gisin and S. Popescu, Phys. Rev. Lett. **83**, 432 (1999).
[13] A. Peres, Phys. Rev. Lett. **77**, 1413 (1996).
[14] J. Bang, S.-W. Lee, H. Jeong, and J. Lee, Phys. Rev. A **86**, 062317 (2012).
[15] E. Magesan, R. Blume-Kohout, and J. Emerson, Phys. Rev. A **84**, 012309 (2011).
[16] *Introduction to Quantum Computation and Information*, edited by H.-K. Lo, S. Popescu, and T. P. Spiller (World Scientific, Singapore, 1998).
[17] The number of vertices for tetra-, hexa-, octa-, dodeca-, and icosahedrons are 4, 8, 6, 20, and 12, respectively. However, half of the points for each polyhedron are located on opposite sites of the other half, except the tetrahedron. Thus, the minimum number of stochastic operations to satisfy the universality condition, represented by each polyhedron, is 4, 4, 3, 10, and 6, respectively. The cases of tetra- and hexahedrons are equivalent.
[18] V. Bužek, M. Hillery, and F. Werner, J. Mod. Opt. **47**, 211 (2000).
[19] S. M. Barnett, J. Mod. Opt. **57**, 227 (2010).
[20] The $\vec{e}_i$ has symmetric and random distributions on an orthogonal plane to $\vec{o}_i$ when $|\vec{e}_i| \ll 1$.
[21] J. N. Damask, *Polarization Optics in Telecommunications* (Springer, Berlin, 2005).
[22] D. F. V. James, P. G. Kwiat, W. J. Munro, and A. G. White, Phys. Rev. A **64**, 052312 (2001).
[23] Although experimental uncertainty of the optical axis is less than 2° in general, we examine up to the case of $\phi_e = 5^\circ$ to clearly

show the $\mathcal{S}_N$. The standard deviation of random errors between $[-\phi_e,\phi_e]$ is proportional to ϕ_e.

[24] See Supplemental Material at http://link.aps.org/supplemental/10.1103/PhysRevA.89.052329 for descriptions of Figs. 2 and 3 in a moving frame.

[25] We repeated QSTs of all the input and output states ten times to analyze the effects of photon counting fluctuations. However, the distribution of reconstructed states is less than the size of a point on the Bloch sphere. Thus we can neglect photon counting fluctuation errors.